Revisiting Near-Marginal Self-Organisation in Fusion Plasmas

G. Dif-Pradalier[1], G. Hornung[2], Y. Asahi[1,3], F. Clairet[1], P.H. Diamond[4], V. Grandgirard[1], X. Garbet[1], Ph. Ghendrih[1], Ö. Gürcan[5], P. Hennequin[5], G. Latu[1], P. Morel[5], R. Sabot[1], Y. Sarazin[1], L. Vermare[5]

[1] CEA, IRFM, F-13108 Saint Paul-lez-Durance, France.
[2] DAP, Ghent University, B-9000 Ghent, Belgium.
[3] JAEA, Wakashiba 178-4, Kashiwa, Chiba 277-0871, Japan.
[4] CMTFO, CER and CASS, University of California, San Diego, USA.
[5] L.P.P. Ecole Polytechnique, Palaiseau, France.

e-mail contact of main author: Guilhem.DIF-PRADALIER@cea.fr

Abstract Large-scale global organisation of turbulence has attracted persistent interest in fusion plasmas as a means to control transport and access improved confinement. It has practical consequences on zonal flow formation and sustainment, on transport levels and on core–edge interplay. We review novel results based on a careful confrontation between flux-driven and gradient-driven gyrokinetics using the GYSELA code and recent experimental data. We present evidence of $\mathbf{E}\times\mathbf{B}$ staircase identification using state-of-the-art ultrafast sweeping reflectometry, discuss its impact on transport near marginality. We also present a clear interplay between core and edge regions of the plasma, discussing key aspects of the controversial 'shortfall problem' in the far-core, near-edge so-called No Man's Land region.

1 Introduction

Global properties of complex systems are often influenced by the dynamics of self-organized mesoscale structures, emerging out of microscopic organisation of turbulent fluctuations. We discuss here manifestations of self-organisation in core plasmas (the $\mathbf{E}\times\mathbf{B}$ staircase) and of edge–core interplay and start assessing their impact on turbulent transport. To this end we compare two modeling frameworks, using the same code GYSELA: flux-driven (the reference case), and gradient-driven (in which self-organisation is constrained). Transport levels, flow and shear organisation and flux-gradient relations change significantly in realistic flux-driven conditions. We also report evidence of edge–core interplay, with edge boundary conditions strongly impacting core turbulence and fluctuation levels.

2 Same code, two frameworks: flux- vs gradient-driven

The usual flux-gradient paradigm [1] relates local values for heat fluxes to local values of the turbulence drive $\eta = L_n/L_T$ (or R/L_T in the case of Ion Temperature Gradient (ITG) instability), *with fixed mean values for the turbulence drive, i.e. fixed mean profiles.* This approach is referred to as "fixed-gradient" or "gradient-driven" (G-D) as opposed to "flux-driven" (F-D) where both fluxes and profiles evolve constantly and are unknown

functions of the dynamics. Here L_x is the gradient length of quantity x, either density n or temperature T. Formally, the flux-driven gyrokinetic equation solved in GYSELA reads:

$$\frac{\mathrm{D}f}{\mathrm{D}t} = \mathcal{C}(f) \, + \, \mathcal{S}(f) \tag{1}$$

where f represents the full ion distribution function, $\mathcal{C}$ the collision operator [2, 3] and $\mathcal{S}$ the source [4]. Switching between a flux- and a gradient-driven framework is done whilst replacing the source term in Eq.(1) by a Krook-type operator that acts as both a source or a sink, depending on the dynamics (the sign of $f - \mathbb{F}_{\text{F-D}}$) and driving a return force with strength γ^K towards the chosen mean profiles $\mathbb{F}_{\text{F-D}}$:

$$\frac{\mathrm{D}f}{\mathrm{D}t} = \mathcal{C}(f) \, - \, \gamma^K \left[f - \mathbb{F}_{\text{F-D}} \left(1 + \frac{\langle\!\langle f - \mathbb{F}_{\text{F-D}} \rangle\!\rangle}{\langle\!\langle \mathbb{F}_{\text{F-D}} \rangle\!\rangle} \right) \right] \tag{2}$$

with $\langle\!\langle \cdot \rangle\!\rangle = \int \mathrm{d}\mathbf{v}\mathrm{d}\theta\mathrm{d}\varphi \, \mathcal{J}_v \mathcal{J} \, \cdot$, $\mathcal{J}_v$ and $\mathcal{J}$ being the velocity and space Jacobians. The last term in Eq.(2) is usual prescription for gradient-driven models [5] so as to prevent overdamping the zonal modes.

In practice, in order to compare flux- and gradient-driven approaches, the target distribution $\mathbb{F}_{\text{F-D}}$ in Eq.(2) is constructed from a saturated flux-driven distribution function. The following procedure is applied that allows GYSELA to mimic usual computations at fixed gradient:

1. a flux-driven computation is run until flux equilibrium. Mean density $n_{\text{F-D}}$, temperature $T_{\text{F-D}}$ and flow profiles are computed;

2. corrugations are removed from the above flux-driven mean profiles resulting in smooth equivalent mean profiles;

3. an equivalent Maxwellian distribution $\mathbb{F}_{\text{F-D}}$ is built from these smooth profiles and imposed in Eq.(2);

4. linear stability is computed for the base state $\mathbb{F}_{\text{F-D}}$. Unstable global modes grow with a maximum growth rate $\gamma_{lin} \sim 6\,10^{-4}\,\omega_{c,i}$;

5. the "spring stiffness" γ^K in Eq.(2) has been varied between $\gamma_{lin}/3$ and $\gamma_{lin}/15$. The results discussed below are qualitatively independent of the precise choice for γ^K. In the following we take $\gamma^K = \gamma_{lin}/10$, consistently with [5];

6. the gradient-driven calculation is compared to the reference flux-driven computation at quasi steady-state for the flows and the fluctuations.

Note that the gradient-driven approach of Eq.(2) contains additional physics as compared to usual gradient-driven approaches. In the latter a scale separation is performed in the equations so that formally the total $f = F_0 + \delta f$ is divided into a background distribution F_0,

fixed in time and a fluctuating part δf. The mean evolution is discarded and so are the nonlinear advection terms that make it evolve. Only δf dynamically evolves and consistency of the performed separation of scales $\delta f/F_0 = o(1)$ has to be checked throughout the computation. In GYSELA, due to the fact that the full distribution function is evolved, the "mean distribution" tends to change and corrugate due to the turbulent dynamics—essentially due to the back-reaction of small turbulence scales on the larger, slower mean scales. Then the Krook-type operator is applied, partly restoring the mean profiles. This gradient-driven approach described by Eq.(2) thus has features of turbulence self-organisation absent when a scale separation is performed. It is thus intermediate between flux-driven and more usual δf global gradient-driven approaches. Differences between F-D and δf G-D approaches are thus expected to be larger that the differences reported below.

3 Core self-organisation: meet the E $\times$ B staircase

A robust feature of flux-driven core plasma self-organisation is the observation in calculations of a self-organised mesoscale structure, referred to as the '$\mathbf{E}\times\mathbf{B}$ staircase' [6, 7]. Narrow regions of corrugated mean temperature profiles and large zonal flow shear (the "risers" of the staircase) appear with typical radial extent $\delta^{\text{flow}} \sim 10\rho_s$, ρ_s being the local Larmor radius. The wider regions in-between (the "treads") are regions of avalanche-mediated transport, and are of typical radial extent Δ. Δ is mesoscale: in-between the local scale length of the turbulence $\ell_c \sim 5 - 8\rho_s$ and a global profile scale length $L_{\{n,T\}} = \{n, T\}/\nabla\{n, T\}$ or the system size $a \geq L_{\{n,T\}}$. Values are reported between $\Delta \sim 30\rho_s$ [6, 7], $\sim 50 - 70\rho_s$ [8] and up to $\sim 100\rho_s$ [9], often with a clear $\rho_\star = \rho_s/a$ dependence [6, 9]. Transport in the 'treads' is reported as strongly nonlocal [6], best described by a Lévy or a Lorentzian kernel of width Δ whilst the 'risers' correspond to regions of weak or permeable transport barriers. Co-located with these barriers are turbulence-driven local corrugations of the pressure profile that drive enduring poloidal flows, an example of synergistic interplay between collisions and turbulence [10]. This structure has also been confirmed in several flux-driven approaches [11, 12, 13, 14, 15, 16, 8, 9]. Further details may be found in the recent overview [17].

Over 200 $\mathbf{E}\times\mathbf{B}$ staircase signatures have recently been experimentally identified [7, 9] in a large variety of plasma parameters in drift-wave turbulence using correlation analysis from ultrafast-sweeping reflectometry [18, 19], over extended regions of core Tore Supra plasmas. Direct observation of mean profile corrugations is uneasy; staircases are thus identified through observation of their successive shear layers, as shown in Fig.1. Many of the expected features of a staircase pattern are confirmed under various experimental plasma conditions in Tore Supra L-mode plasmas. The key signatures are: a robust pattern of quasi-regularly spaced local reductions of the radial correlation length L_{coh} of turbulent fluctuations, a sudden variation of their tilt across the successive staircase shear layers, no correlation to low-order q rationals and a shear flow layer width that scales with the local sound gyroradius $\sim 11\rho_s$, close to expected δ^{flow} values [7, 20]. New features also stand

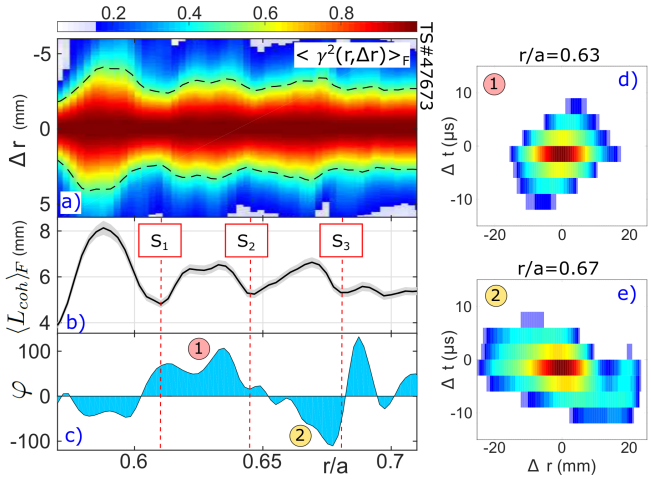

Figure 1: Successive staircase shear layers appear experimentally as quasi-regular local contractions of the coherence and through differential eddy tilting. See details in Ref.[9]

out from the compiled database of staircase observations. These are further discussed in Ref.[9]. Interestingly, staircase observation seems to depend on the free energy source: observed in near-marginal ion drift-wave turbulence, staircases seem to disappear in electron drift-wave dominated regimes. An increased permeability of transport barrier with plasma size $\rho_\star = \rho_s/a$ is also found, suggesting an unfavourable scaling of transport with $\rho_\star$, a being the minor radius. Of concern for large experiments, this observation opens new routes to understanding *gyro-Bohm breaking through micro-barrier permeability*. These results provide a relatively inexpensive and reliable means to characterise flow shear with high space and time resolution that has broad applicability to characterising transport, barrier onset and dynamics as well as transitions to regimes of improved confinement.

4 Self-organisation near criticality: impact on transport

It is important to assess the impact of staircase organisation on transport. Thus, we first compare [21] both flux- and gradient-driven approaches Eqs(1) and (2) in the banana regime. The striking feature in Fig.2 is that the staircase pattern that exists and endures in the flux-driven computation is rapidly [in less than a millisecond] damped away and ultimately lost in the gradient-driven approach. The strong inhomogeneities in the mean shear, poloidal flow and temperature that have spontaneously appeared in the flux-driven case give way to a more homogeneous turbulence with a strong isotropisation of the fluctuations and of the flow structure. The PDF of the fluctuations is more skewed in the flux-driven case and has as expected a significantly broader tail. The randomisation of the fluctuations across the radius with no large-scale long-lived mean component in gradient-driven steady-state contrasts with the flux-driven strongly organised flow and avalanche pattern. A follow-on question is of course the impact that such discrepancies might generate on transport.

To this end, we compare in Fig.3 the turbulent heat fluxes in flux- and gradient-driven regimes, respectively $Q^{\text{turb}}_{\text{F-D}}$ and $Q^{\text{turb}}_{\text{G-D}}$. In both approaches the turbulence drive R/L_T varies with radius so that R/L_T varies between 4 and 8 between $r/a = 0.3$ and 0.7. The heat

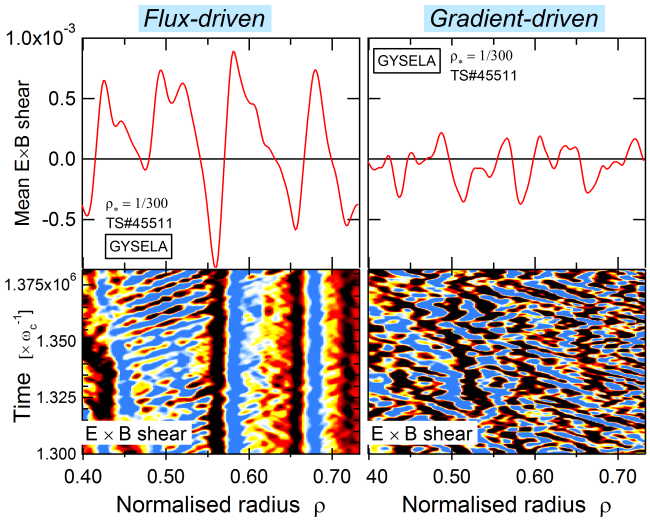

Figure 2: Comparison of flux- and gradient-driven computations: no perennial structures endure in the gradient-driven approach, structures are more isotropic, their propagation direction is more random, mean components are vanishing and the staircase pattern is lost.

fluxes in Figs.3 and 4 are the time-averaged values during $0.5ms$ of the heat fluxes at different radial locations, at flux equilibrium. The shaded regions are the temporal fluctuations during that time. We superpose in Fig.4 the PDF of staircase-related corrugations of the mean temperature profile as a function of R/L_T, thus asking in what region of turbulence drive is the staircase most likely to be found. Let us call 'linear threshold' the turbulence drive for which unstable modes start growing—in Figs.3 and 4, $R/L_T^{\rm lin} \approx 3.5$. Following Ref.[1] let us call 'non-linear threshold' the turbulence drive at which the turbulent heat flux suddenly increases—'stiffness' is the slope of that increase—and 'marginality' (or 'criticality') the turbulence drive at which the turbulent heat flux dominates over its neoclassical counterpart. The turbulent regime starts above marginality. Similarly, the 'Dimits upshift' is the region of turbulence drive in-between linear and non-linear thresholds. Several features stand out:

- as expected, in gradient-driven modeling a clear Dimits shift exists associated to fluctuating zonal flows that lead to a low level of turbulent transport. Stiffness is large at marginality and a smooth, monotonically increasing flux-gradient relation is found;

- in contrast in flux-driven modeling the Dimits shift (if any) is strongly reduced and turbulent transport there is significantly larger than in the G-D case. This result still holds at low collisionality [22]. However once in the turbulent regime, despite the increase of R/L_T the heat flux does not further increase owing to the mean flow regulation of transport as a result of the $\mathbf{E} \times \mathbf{B}$ staircase. Not detailed here, it is worth noticing that the flux-gradient relation in the flux-driven regime is multivalued [23] (non-monotonic) where the staircase exists, as may be expected for its formation through negative viscosity arguments, i.e. heat accumulation despite increased drive;

- in-between the onset of the F-D turbulent regime and the beginning of the G-D turbulent regime, the F-D heat flux in Fig.3 is strongly intermittent. Even though it

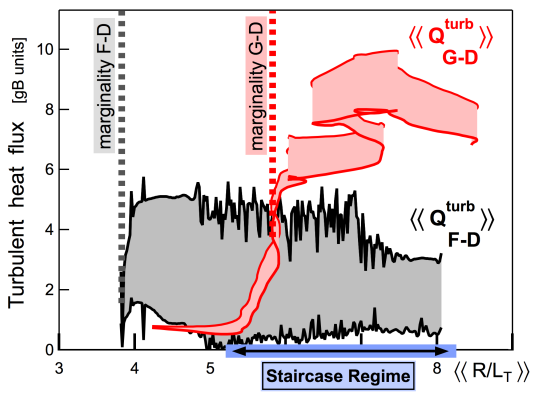

Figure 3: Flux- and gradient-driven turbulent heat fluxes significantly differ near marginal stability.

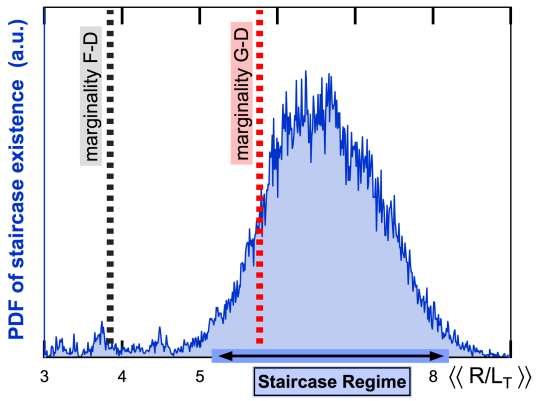

Figure 4: The $\mathbf{E} \times \mathbf{B}$ staircase is a near-marginal pattern: it forms and endures in a precise region of R/L_T drive.

does not change much in amplitude when entering the staircase regime, it changes in nature: through its shear layers, the staircase now radially organises the heat flux and controls its dynamics;

- the staircase is a near-marginal pattern: it resides in the low-heating limit of flux-driven forcing [7, 8]. As it requires turbulence activity to nucleate and endure, it locates close but certainly above the onset of F-D turbulent regime. Interestingly, though this may be fortuitous, its seems to exist close to G-D marginality.

The essential differences of a F-D regime as compared to a G-D framework are: the sustainment of a significant turbulent activity arbitrarily close to linear threshold, strong intermittence (its variation with R/L_T is not presented here) and at larger turbulence drives the onset of the $\mathbf{E} \times \mathbf{B}$ staircase. Entering the staircase regime, the system transitions from being randomly organised everywhere and regulated by fluctuating zonal flows to being strongly organised through mean flow patterning (the onset of the weak staircase transport barriers). In the staircase regime flux-driven transport is reduced by a factor of 2 to 3 as compared to the gradient-driven prediction where no staircase patterning occurs.

5 Edge–core interplay

The previous sections were mostly focused on core plasma self-organisation. We recently upgraded GYSELA to account close to the outer edge ($r/a \geq 1$) for Scrape-Off-Layer-like (SOL) boundary conditions. This allows us to investigate in flux-driven regimes how core and edge may interplay. We diagnose this question whilst investigating the radial behaviour of turbulent fluctuations.

We focus here on the impact of an edge turbulent activity on the global core–edge organisation. To this end, we run two F-D computations in Figs.5 and 6, at flux equilibrium,

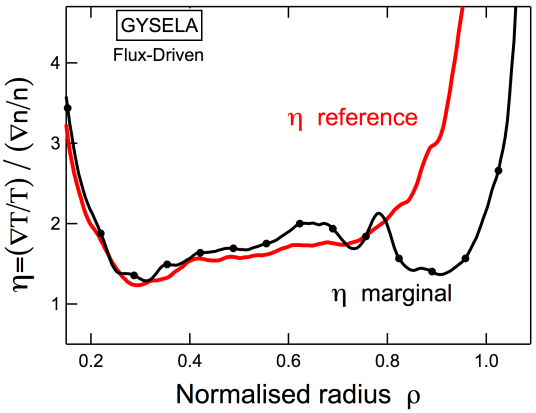

Figure 5: By changing L_n, two steady-state flux-driven η profiles are compared.

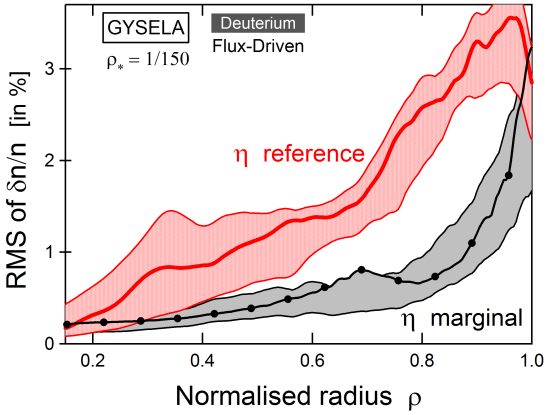

Figure 6: Edge turbulence activity impacts flux-driven transport levels everywhere.

only changing $\eta = L_n/L_T$ close to the edge: from $r/a = 0.7$ to 1. L_T evolves self-consistently, L_n is fixed and allows to scan η. The 'reference' case is a near-marginal instability profile η up to $r/a \approx 0.7$ and unstable profiles beyond $r/a \geq 0.7$. The 'marginal' case has very similar profiles up to $r/a \approx 0.7$, remains near-marginal up to $r/a = 1$ and becomes unstable in the SOL. Remarkably the density fluctuation levels are much lower in the marginal case, even below $r/a \leq 0.7$ where both gradient scales lengths η are comparable. Two main conclusions seem to hold: as η always increases close enough to the edge (i) spreading of near-marginal core turbulence seems of limited practical importance as compared to the spreading of more strongly driven edge turbulence [24], (ii) core–edge self-organisation is global so that modeling choices for edge and SOL are not innocuous for even deep core transport properties.

6 Conclusion

Self-organisation in core plasmas has led to predicting the $\mathbf{E} \times \mathbf{B}$ staircase, which has since been confirmed by other models and found experimentally through correlation of density fluctuations. This global pattern deeply modifies near-marginal transport levels and stiffness. Edge and SOL boundary conditions are important contributors as well to core transport as large-scale self-organisation through edge–core interplay strongly impacts predicted transport and fluctuation levels across the entire plasma volume.

Acknowledgments

This work has been carried out within the framework of the EUROfusion Consortium and the French Research Federation for Fusion Studies and has received funding from the Euratom research and training programme 2014-2018 under grant agreement No 633053. We benefited from HPC re-

sources from GENCI, CCRT-TGCC and IFERC.

References

[1] A. M. Dimits, et al. *Physics of Plasmas*, 7(3):969–983, 2000.

[2] G. Dif-Pradalier, et al. *Physics of Plasmas*, 18(6):062309, 2011.

[3] D. Estève, et al. *Physics of Plasmas*, 22(12), 2015.

[4] Y. Sarazin, et al. *Nuclear Fusion*, 50(5):054004, 2010.

[5] B. F. McMillan, et al. *Physics of Plasmas*, 15(5):052308, 2008.

[6] G. Dif-Pradalier, et al. *Phys. Rev. E*, 82(2):025401(R), Aug 2010.

[7] G. Dif-Pradalier, et al. *Phys. Rev. Letters*, 114(085004), 2015.

[8] F. Rath, et al. *Physics of Plasmas*, 23(5), 2016.

[9] G. Hornung, et al. *Nucl. Fusion*, submitted, 2016.

[10] G. Dif-Pradalier, et al. *Physical Review Letters*, 103(6):065002, 2009.

[11] M. Nakata and Y. Idomura. *Nucl. Fusion*, 53:113039, 2013.

[12] Y. Kosuga, et al. *Physics of Plasmas (1994-present)*, 21:055701, 2014.

[13] L Villard, et al. *Plasma Physics and Controlled Fusion*, 55(7):074017, 2013.

[14] C Norscini, et al. *Journal of Physics: Conference Series*, 561(1):012013, 2014.

[15] Ph. Ghendrih, et al. *Journal of Physics: Conference Series*, 561(1):012008, 2014.

[16] K. Imadera, et al. *4th APTWG International Conference, Fukuoka, Japan*, 2014.

[17] G. Dif-Pradalier, et al. *Plasma Phys. Control. Fusion*, submitted, 2016.

[18] F. Clairet, et al. *Review of Scientific Instruments*, 82(8):083502, 2011.

[19] G. Hornung, et al. *Plasma Physics and Controlled Fusion*, 55(12):125013, 2013.

[20] A. Fujisawa. *Nuclear Fusion*, 49(1):013001 (42pp), 2009.

[21] X. Garbet, et al. *Nuclear Fusion*, 39(11Y):2063, 1999.

[22] Z. Lin, et al. *Phys. Rev. Letters*, 83(18):3645, November 1999.

[23] P. H. Diamond, et al. *Phys. Rev. Lett.*, 78:1472–1475, Feb 1997.

[24] X. Garbet, et al. *Nuclear Fusion*, 34(7):963–74, 1994.